Islamic Azad University

Journal of
Optoelectronical Nanostructures

Autumn 2023 / Vol. 8, No. 4

Research Paper

Design of a Three-Element Apochromatic Lens to Correct Axial Chromatic Aberration at UVA Wavelength Band

Ali Rezaei-Latifi *
Physics Department, Faculty of Sciences, University of Hormozgan, Bandar Abbas, *Iran*

Received: 11 Agu. 2023
Revised: 13 Oct. 2023
Accepted: 5 Dec. 2023
Published: 15 Dec. 2023

Use your device to scan and read the article online

Keywords:
Airy Radias,
Apochromat,
Secondary Spectrum,
Spot Diagram

Abstract:

Apochromat is usually designed for color correction in the range of the visible spectrum. But to correct the chromatic aberration of optical systems outside the visible spectrum, apochromatic lens in the same spectral band should be used. In this work, firstly, a three-element apochromatic lens in the UVA spectral region is pre-designed and optimized by spherical lenses with suitable glasses. The primary spherical aberration of this apochromat is almost zero and its tertiary spectrum has a small value of 2.558 microns. Nevertheless, the spherical aberration of higher orders causes the RMS radius in the spot diagram to be several times larger than the Airy radius. Then, by selecting aspheric surfaces and re-optimizing the system, a spherical aberration-free apochromatic with a small tertiary spectrum is designed. In this last design, the RMS radius is smaller than the Airy radius, so almost all points are located inside the Airy disk. This lens can be used to correct chromatic aberration in UVA imaging spectrometers and cameras.

Citation: Ali Rezaei-Latifi.
Design of a three-element apochromatic lens to correct axial chromatic aberration at UVA wavelength band. **Journal of Optoelectronical Nanostructures. 2023; 8 (4):63- 81. DOI: 10.30495/JOPN.2024.31998.1291**

***Corresponding author:** Ali Rezaei-Latifi
Address: Physics Department, Faculty of Sciences, University of Hormozgan, Bandar Abbas, *Iran* **Tell:** 09171831502 **Email:** r_latifi@hormozgan.ac.ir

1. INTRODUCTION

A lens that can correct the effects of the secondary spectrum is called an apochromat. The secondary spectrum in visible light is defined as the distance between the d (yellow) line focus and the common focal point of C (red) and F(blue) lines. An achromat brings the focus of F and C to the same point and an apochromat usually reduces secondary color by bringing three spectral lines of C (red), d (yellow), and F (blue) to a common focus [1-3]. Color aberration correction can be extended to an invisible spectrum such as (ultraviolet) UV by bringing two or more wavelengths to the same focus.

UV radiation covers the wavelength range of 100-400 nm and is divided into three bands: UVA (315-400 nm), UVB (280-315 nm), and UVC (100-280 nm) [4-5]. The solar spectrum at sea level contains plenty of UVA light for imaging, but virtually no shortwave-UV(UVB and UVC) light. Therefore outdoor imaging using reflected sunlight is possible in the UVA band, but shortwave-UV imaging requires an active illumination source [6]. Ultraviolet imaging has a wide variety of scientific, industrial, and medical applications [7], for example in forensics [8], digital imaging [9], power equipment inspection [10], Monitoring treatment programs [11], remote sensing [12,13] and in astronomy[14].

Recent advances in silicon-based image sensors have opened opportunities for imaging in a broad wavelength ranging from deep UV to about 1100 nm in the near-infrared [15,16]. There are currently optical designs that are corrected from near-IR to near-UV but are not suited for use for the shorter wavelengths in the UVA waveband ranging from 315 nm up to about 350 nm. The reason for this defect is either due to a lack of optical correction or a lack of transparency, or both[16]. Broadband hyperspectral imaging in this spectral region is challenging due to strong chromatic aberrations inherent in UV systems [17].

In this work, at first, a three-element apochromatic with a focal length of 100 mm to correct axial chromatic aberration at the UVA wavelength band is designed**.** Then, using aspherical surfaces, its spherical aberration is corrected. The rest of the paper is organized as follows. Section 2 describes the methods and materials used to three-element apochromat**.** The result of the calculations is analyzed in Section 3. The final section provides the conclusion.

2. MATERIAL AND METHOD

At first, we obtain the formulas needed for the pre-design of apochromat in the UV spectral region. We consider three different wavelengths at the beginning, λ_b, middle λ_m, and end λ_e of the UVA band, and in the design of the apochromat, we try to bring the focus of these three wavelengths to a common point. In the first step, by bringing two wavelengths λ_b and λ_e to a common focal point, we obtain the necessary equations to counteract the deleterious effects of the primary axial focus.

The power of a thin lens φ at wavelength λ is given by [1]:

$$\boldsymbol{\varphi = (n-1)(C_1 - C_2)} \quad \textbf{(1)}$$

where C_1 and C_2 are the curvatures of the two lens surfaces. By taking the derivative of equation (1) with respect to the refractive index we obtain:

$$\boldsymbol{d\varphi = (C_1 - C_2)dn} \quad \textbf{(2)}$$

If we assume $dn = (n_b - n_e)$ then

$$\boldsymbol{d\varphi = (C_1 - C_2)(n_b - n_e)} \quad \textbf{(3)}$$

If we define the Abbe number for the UVA spectral region as follows:

$$\boldsymbol{v = \frac{n_m - 1}{n_b - n_e}} \quad \textbf{(4)}$$

Then

$$\boldsymbol{d\varphi = \frac{\varphi_m}{v} = (\varphi_b - \varphi_e)} \quad \textbf{(5)}$$

Now we consider a triplet lens consisting of three suitable glasses in the ultraviolet region. The three types of glass we choose here are Calcium Fluoride, Silica, and Quartz. Calcium Fluoride has excellent transmission properties in both ultraviolet and infrared, making it valuable for instrumentation purposes. Furthermore, its partial dispersion characteristics are such that it can be combined with optical glass to form a lens system without a secondary spectrum. Its physical properties are not outstanding because it is soft and fragile and has a crystal structure which sometimes makes polishing difficult. In exposed applications, it is best to place Calcium Fluorite between the glass elements to protect their surfaces [18-20]. Silica is widely used in various optical instruments [21-25]. This material is known to have high transmittance in the visible and UV to wavelengths as short as 170 nm. It is also nominally free of fluorescence and practically free of coloration when exposed to ionizing radiation [26]. Quartz glass has an extraordinarily high optical transmissivity for ultraviolet light. Due

to its low coefficient of thermal expansion, Quartz glass can resist very high operating temperatures [27]. The optical power of this thin triple lens is equal to:

$$\boldsymbol{\varphi = \varphi_Q + \varphi_C + \varphi_S} \quad \textbf{(6)}$$

that indices Q, C, and S represent Quartz, Calcium Fluoride, and Silica glasses, respectively. The derivative of the above equation gives:

$$\boldsymbol{d\varphi = d\varphi_Q + d\varphi_C + d\varphi_S} \quad \textit{(7)}$$

Substituting from equation (5):

$$\mathbf{d\varphi = \frac{(\varphi_m)_Q}{v_Q} + \frac{(\varphi_m)_C}{v_C} + \frac{(\varphi_m)_S}{v_S}} \quad \textbf{(8)}$$

By setting $d\varphi = 0$, we force the light with λ_b and λ_e wavelengths together.

Now, in order to get the formula to bring the focus of light with wavelength λ_m and λ_e to a common point, we return to equation (2) and take dn as $(n_m - n_e)$. Therefore, for a singlet, we will have:

$$\boldsymbol{d\varphi = (C_1 - C_2)(n_m - n_e)} \quad \textit{(9)}$$

We define partial dispersion for the end half of the UVA spectrum as follows

$$\boldsymbol{p_{me} = \frac{n_m - n_e}{n_b - n_e}} \quad \textit{(10)}$$

By combining relations (1), (4), (9), and (10) we get the power difference between the light in the middle and the end of the spectrum:

$$\mathbf{d\varphi = \left(\frac{p_{me}}{v}\right)\varphi} \quad \textbf{(11)}$$

The use of this equation for the thin layer introduced above is as follows:

$$\boldsymbol{d\varphi = \left(\frac{p_{me}}{v_Q}\right)_Q \varphi_Q + \left(\frac{p_{me}}{v_C}\right)_C \varphi_C + \left(\frac{p_{me}}{v_S}\right)_S \varphi_S} \quad \textit{(12)}$$

By setting $d\varphi = 0$, we force the light with λ_m and λ_e wavelengths together. Therefore, for the apochromatic mentioned above with a certain power φ, we have the following three constraints:

 DOI: 10.30495/JOPN.2024.31998.1291

$$\begin{cases} \varphi = \varphi_Q + \varphi_C + \varphi_S \\ 0 = \frac{\varphi_Q}{v_Q} + \frac{\varphi_C}{v_C} + \frac{\varphi_S}{v_S} \\ 0 = (\frac{p_{me}}{v})_Q \varphi_Q + (\frac{p_{me}}{v})_C \varphi_C + (\frac{p_{me}}{v})_S \varphi_S \end{cases} \quad (13)$$

By solving the above equations, we get the power of each of the three apochromatic elements in terms of the total power :

$$\varphi_Q = \frac{v_{Q(}\Delta p_{SC})\varphi}{\Delta} \quad (14)$$

$$\varphi_C = \frac{v_C(\Delta p_{QS})\varphi}{\Delta} \quad (15)$$

$$\varphi_S = \frac{v_S(\Delta p_{CQ})\varphi}{\Delta} \quad (16)$$

In the above equations, the symbol Δ is:

$$\Delta = v_Q \Delta p_{SC} + v_C \Delta p_{QS} + v_S \Delta p_{CQ} \quad (17)$$

Where $\Delta p_{SC} = (p_{me})_S - (p_{me})_C$ and so on.

Zemax optical software is used to calculate the refractive index of glasses and to optimize the apochromatic. Zemax uses different formulas to calculate the refractive index. Here, the following equation, which is known as Schott's equation, is selected to calculate the refractive index of glasses[18, 28]:

$$n^2(\lambda) = a_0 + a_1\lambda^2 + \frac{a_2}{\lambda^2} + \frac{a_3}{\lambda^4} + \frac{a_4}{\lambda^6} + \frac{a_5}{\lambda^8} \quad (18)$$

Where the constants (a_0 , a_1 , a_2 , etc.) are derived for each material by substituting known index and wavelength values and solving the resulting simultaneous equations for the constants [18].

The results of the refractive index, Abbe number, and partial dispersion of apochromatic elements are shown in Table 1.

TABLE 1
Properties of apochromatic glasses

Glass	n_b	n_m	n_e	v	p_{me}
Quartz	1.573694	1.564117	1.557684	35.235290	0.401811
CaF_2	1.451361	1.445699	1.441854	46.881140	0.403337
Silica	1.483901	1.475676	1.470116	34.506782	0.403337

Here we want to design an apochromat with a focal length of 100 mm. Therefore, $\varphi = 0.01\ (mm)^{-1}$. According to equations 14 to 16 and Table 1, we obtain the following values for the power and focal length of each of the apochromatic components:

$$\boldsymbol{\varphi_Q = 0.019724\ (mm)^{-1} \rightarrow f_Q = 50.699\ mm} \quad \textbf{(19)}$$

$$\boldsymbol{\varphi_C = 0.036341\ (mm)^{-1} \rightarrow f_C = 27.517 mm} \quad \textbf{(20)}$$

$$\boldsymbol{\varphi_S = -0.046065\ (mm)^{-1} \rightarrow f_S = -21.708\ mm} \quad \textbf{(21)}$$

Now that the powers of the three elements are found, the next step is to determine the initial curvatures for these lenses. We place the lens with Calcium Fluorite glass between two other lenses to protect its surfaces and also assume that this lens is equiconvex (Fig. 1). Therefore, according to the thin lens power formula:

$$\boldsymbol{\varphi_C = ((n_m)_C - 1)(C_3 - C_4)} \quad \textbf{(22)}$$

$$\boldsymbol{C_4 = C_5 = -C_3 \rightarrow\ C_3 = \frac{\varphi_C}{2((n_m)_C - 1)} = 0.040768 = C_2}$$

$$\boldsymbol{Or\ R_3 = \frac{1}{C_3} = 24.529\ mm = R_2 = -R_4 = -R_5} \quad \textit{(23)}$$

$$\boldsymbol{\varphi_Q = ((n_m)_Q - 1)(C_1 - C_2)}$$

$$\boldsymbol{0.019724 = (1.564117 - 1)(C_1 - 0.040768) \rightarrow C_1 = 0.075732}$$

$$\boldsymbol{\rightarrow\ R_1 = 13.204\ mm} \quad \textbf{(24)}$$

$$\varphi_S = ((n_m)_S - 1)(C_5 - C_6) \quad (25)$$

$$-0.046065=(1.475676-1)(-0.040768-C_6)$$

$$\rightarrow C_6 = 0.056073 \rightarrow R_6=17.833\ mm \quad (26)$$

To see the results of the pre-design and optimization of the lens, we enter the values obtained above according to Table 2 in Zemax software. Considering that the power formulas of the thin lens used above are for when there is air on both sides of the lens, therefore, we have put a small distance of 0.001 mm in the pre-design and then removed this distance after optimization. It should be noted that the image screen is placed at the back focal point.

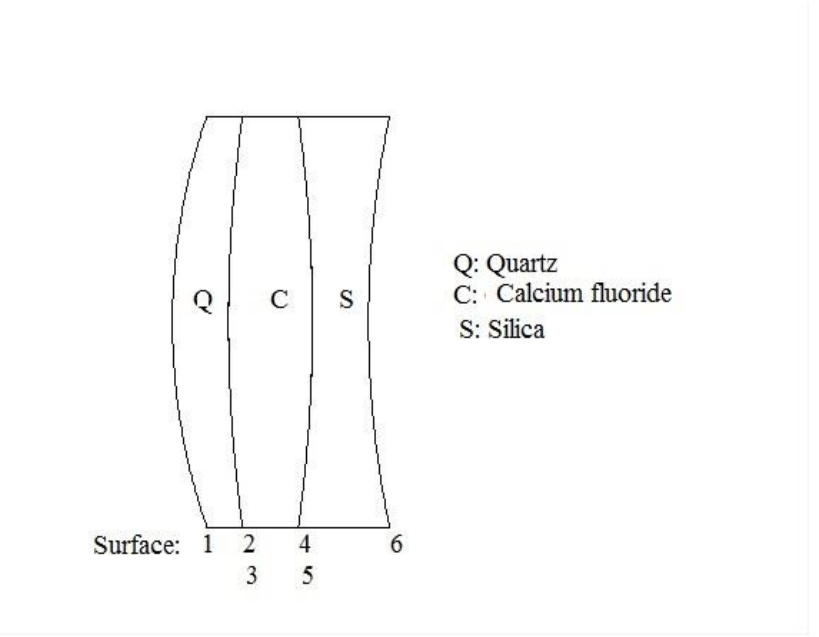

Fig. 1. Arrangement of apochromatic components

TABLE 2
Thin apochromatic surface data.

surface	Radius	Thickness	Glass	Semi-Diameter	Conic
0(OBJECT)	Infinity	Infinity		0	0
1	13.206	0	QUARTZ	5	0
2	24.529	1.000E-003		5.066	0
3	24.529	0	CAF2	5.066	0
4	-24.529	1.000E-003		5.220	0
5	-24.529	0	SILICA	5.220	0
6	17.833	100.034		5.048	0
7(IMAGE)	Infinity	-		0.504	0

3. RESULTS

Figure 2 shows the chromatic shift diagram in the thin (no thickness) apochromatic preliminary design. In this diagram, the vertical axis is the wavelength, and the horizontal axis is the distance of the focal point in each wavelength from the focal point of the primary wavelength, λ_m. The maximum focal shift range, that is, the tertiary spectrum, is 3.3771 μm. In this lens, the focus of wavelengths λ_b, λ_m, and λ_e are almost the same. Apochromat without thickness has no physical reality, and therefore, here we consider 2 mm, 3 mm, and 2 mm thicknesses for Quartz, Calcium Fluoride, and Quartz glasses, respectively. Now we can see that the color correction has decreased a lot so that the maximum range of focal change has reached 1141.4156 (Fig. 3). Therefore, in order to correct the axial chromatic aberration, we optimize the system as described below.

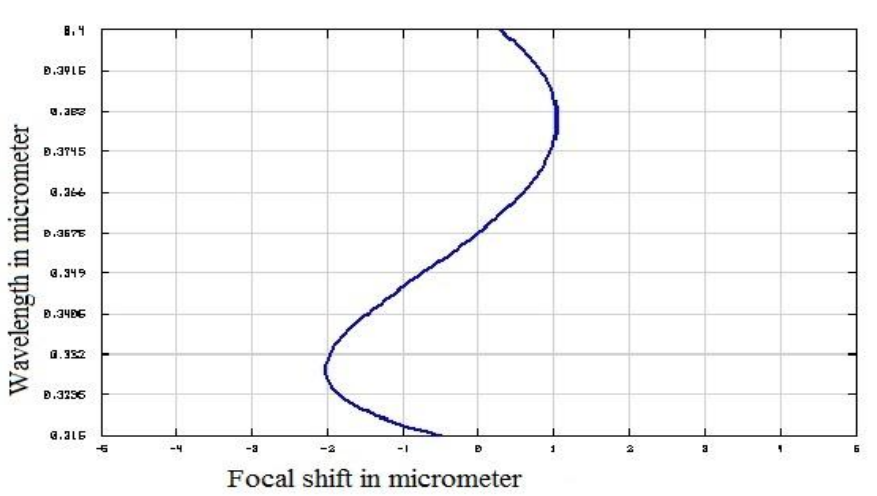

Fig. 2. Thin apochromatic chromatic shift in micrometer.

By changing the radii of the lens surfaces and using appropriate operands in the merit function editor of Zemax software (Table 3), we bring three lights with wavelengths λ_b, λ_m, and λ_e to a common focus. The value of the merit function after optimization is equal to 4×10^{-8}, which is a small number and indicates that the current values of various operands after optimization are very close to the target values according to their weight. The value of the merit function is calculated from the following equation

$$\mathbf{MF^2} = \frac{\sum \mathbf{W_i(V_i - T_i)^2}}{\sum \mathbf{W_i}} \quad \textbf{(27)}$$

where w_i is the weight of operand i, T_i is the target value and V_i is the current value of the operand i, respectively [29].

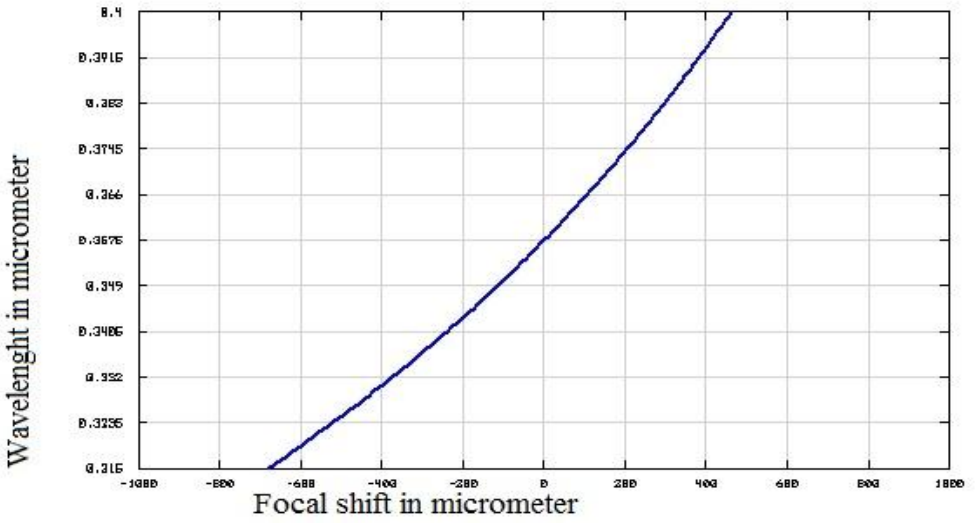

Fig. 3. Focal shift in the real design before optimization.

TABLE 3
Merit function editor for apochromat optimization.

Operand	Wave	Surf#1	Surf#2	P_x	P_y	Op#1	Op#2	Target	weight	Value
EFFL	λ_m	-	-	-	-	-	-	100	1	100
EFLY	λ_m	1	2	-	-	-	-	50.700	0	61.382
EFLY	λ_m	3	4	-	-	-	-	27.517	0	21.526
EFLY	λ_m	5	6	-	-	-	-	-21.708	0	-17.887
PARR	λ_b	7	-	0	0.1	-	-	0	0	4.05E-8
PARR	λ_m	7	-	0	0.1	-	-	0	0	9.44E-16
DIFF	-	7	-	-	-	5	6	0	70	4.05E-8
PARR	λ_m	7	-	0	0.1	-	-	0	0	9.44E-16
PARR	λ_e	7	-	0	0.1	-	-	0	0	6.40E-8
DIFF	-	7	-	-	-	8	9	0	70	-6.40E-8
SPHA	λ_m	-	-	-	-	-	-	0	100	-4.07E-12

 DOI: 10.30495/JOPN.2024.31998.1291

Figure 4 shows the three-dimensional layout of the apochromat and Table 4 shows the lens surface data after system optimization. After optimization, the radii of the lens surfaces are variated according to Table 2. Changing the radius of the lens surfaces changes the power of each of the apochromatic components, but the total apochromatic power remains constant.

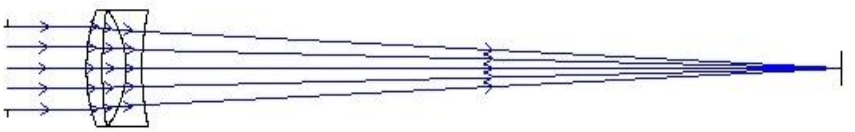

Fig. 4. The 3D layout of the three-element apochromat after optimization using spherical surfaces.

TABLE 4
Lens surface data after system optimization with spherical lenses.

surface	Radius	Thickness	Glass	Semi-Diameter	Conic
0(OBJECT)	Infinity	Infinity		0	0
1	20.457	2	QUARTZ	7 U	0
2	48.231	0		7 U	0
3	48.231	3	CAF2	7 U	0
4	-11.747	2		7 U	0
5	-11.747	0	SILICA	7 U	0
6	32.557	88.143		7 U	0
7(IMAGE)	Infinity	-		7 U	0

Figure 5 shows the focal shift diagram in the designed real apochromat after system optimization. After optimization, the focus of wavelengths λ_b, λ_m, and λ_e completely coincide with each other, and the tertiary spectrum decreases to 2.558 microns. At the same time, in this design, we tried to reduce the third-order spherical aberration of Seidel w_{040} as much as possible. Table 3 shows that w_{040} has decreased to the value of $-4 \times 10^{-12}\lambda_m$, that is, almost zero. Figure 6 shows the spot diagram for the middle wavelength λ_m. Although the Root-Mean-Square (RMS) radius is a small value of 19.960 microns, not all points are located in the Airy disk. When we reduced the primary spherical aberration to almost zero and there were no other aberrations, there is a question as to why all the points are not included in the Airy disk. Further investigations showed that the presence of fifth and seventh higher-order spherical aberration caused all points in the spot diagram not to fall into the Eiry disk. By using the aspherical surfaces, it can almost eliminate different orders of spherical aberration simultaneously. Aspherical lenses are less used in optical systems than spherical lenses due to the cost and difficulties in manufacturing. However, this view is now changing due to the rapid development of precision engineering [30].

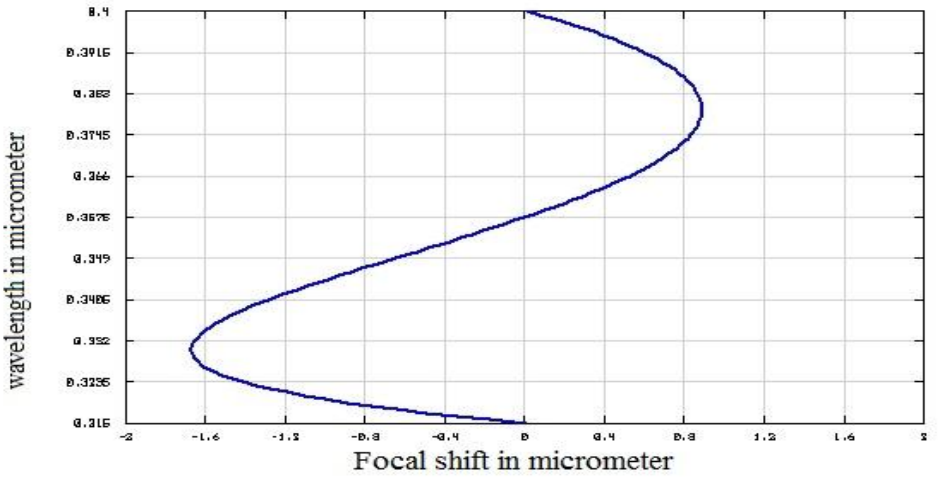

Fig. 5. Focal shift in the real apochromat design after optimization.

 DOI: 10.30495/JOPN.2024.31998.1291

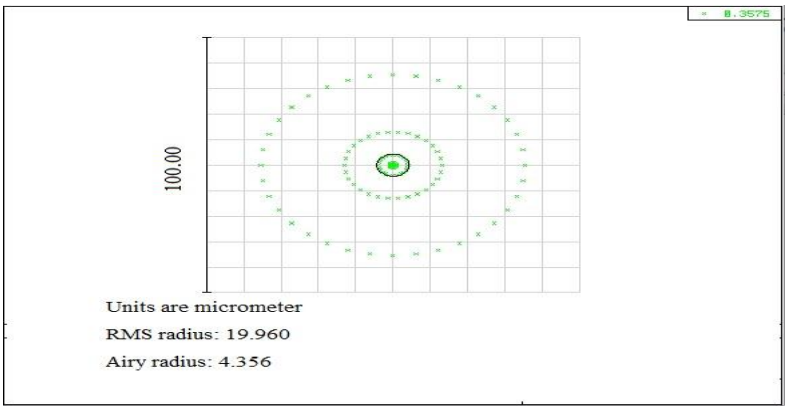

Fig. 6. Spot diagram of the real apochromat with spherical lenses.

Table 5 indicates lens surface data after system optimization with aspherical lenses. According to the conic constant values in Table 5, surfaces 1, 4 (or 5), and 6 are hyperbola, and surface 2 (or 3) is an oblate ellipse. With this data, the RMS radius of the lens decreases to 2.594 microns, which is smaller than the radius of the Airy disk (4.491 microns), so all the rays in the image plane are located inside the Airy disk (Figure 7). Other metrics determining the quality of the image such as ray fan plots (not shown) show that the spherical aberration is almost completely removed. Figure 8 shows the focal shift diagram in the designed real apochromatic with aspherical lenses. For this apochromat, the tertiary spectrum is 2.528 microns.

TABLE 5
Lens surface data after system optimization with aspherical lenses.

surface	Radius	Thickness	Glass	Semi-Diameter	Conic
0(OBJECT)	Infinity	Infinity		0	0
1	23.360	2	QUARTZ	7 U	11.691
2	74.379	0		7 U	-40.647
3	74.379	3	CAF2	7 U	-40.647
4	-11.375	2		7 U	1.027
5	-11.375	0	SILICA	7 U	1.027
6	41.833	89.487		7 U	54.880
7(IMAGE)	Infinity	-		7 U	0

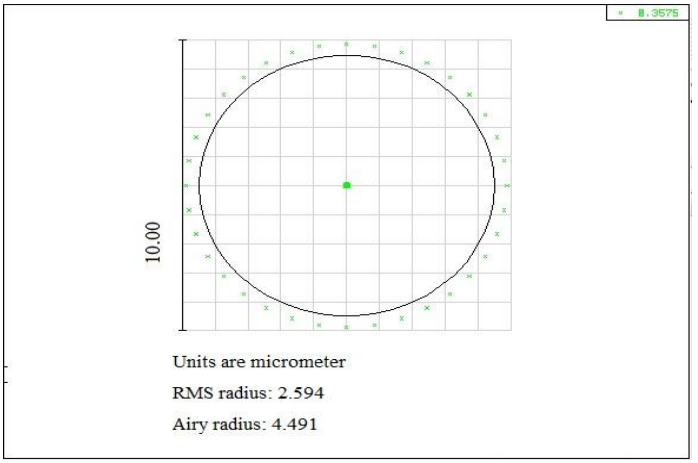

Fig. 7. Spot diagram of the real apochromat with aspherical lenses.

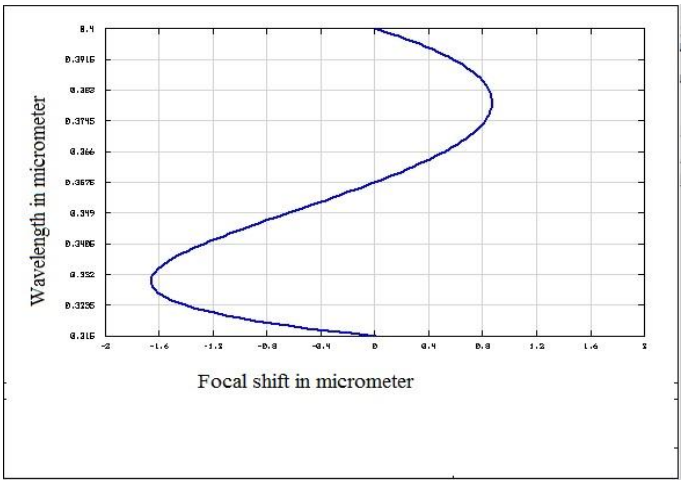

Fig. 8. Focal shift in the real apochromat with aspherical lenses.

4. CONCLUSION

In this paper, two types of apochromats were designed at the UVA wavelength band. The first apochromat was pre-designed and optimized by using spherical surfaces and suitable glasses. In the design of the second apochromat, the same glasses were used, but in the optimization of the system, it was left free so that the lens surfaces could be aspherical. In the optimization of this second design, the spherical surfaces of the lenses were changed to hyperbolic and elliptical surfaces. In both designs, the effects of the secondary spectrum were well corrected and the focus of the wavelengths of the beginning, middle, and end of the spectrum was brought to one point. In both designs, the tertiary spectrum is a small value. In the first design, although the primary spherical aberration is almost zero, the metrics determining the quality of the image such as spot diagrams and ray fan plots showed that higher-order spherical aberrations were almost noticeable. In the second design, Seidel's primary spherical aberration and higher orders were almost all removed. Aspherical lenses are used less than spherical lenses due to cost and manufacturing problems. However, this trend is currently changing due to the rapid development of precision engineering.

References

[1] J. M. Geary, *Introduction to lens design: with practical ZEMAX examples*, Richmond, VA, USA: Willmann-Bell, 2002.
Available:https://www.amazon.com/Introduction-Lens-Design-Practical Examples/dp/0943396751#detailBullets_feature_div

[2] R. Kingslake, R. B. Johnson, *Lens design fundamentals*, academic press, 2010.
Available: https://www.sciencedirect.com/book/9780123743015/lens-design-fundamentals

[3] J. Laatikainen, *Design of Apochromatic Lenses*, MS thesis, Itä-Suomen yliopisto, 2020.
Available:
https://erepo.uef.fi/bitstream/handle/123456789/22245/urn_nbn_fi_uef-20200556.pdf

[4] A. Sample, B. Zhao, C. Wu, S. Qian, X. Shi, A. Aplin,Y. He, *The autophagy receptor adaptor p62 is up-regulated by UVA radiation in melanocytes and in melanoma cell,*. Photochemistry and photobiology, 94(3) (2018, July) 432- 437.
Availabe: **https://doi.org/10.1111/php.12809**

[5] L. R. Sklar, F. Almutawa, H. W. Lim, I. Hamzavi, *Effects of ultraviolet radiation, visible light, and infrared radiation on erythema and pigmentation: a review*, Photochemical & Photobiological Sciences, 12(1) (2012, December) 54-64.
Available: https://link.springer.com/article/10.1039/c2pp25152c

[6]https://www.photonics.com/Articles/Ultraviolet_Reflectance_Imaging_Applications/a32169

[7] T. C. Wilkes, A. J. McGonigle, T. D. Pering, A. J. Taggart, B. S. White, R. G. Bryant, J. R, Willmott, *Ultraviolet imaging with low-cost smartphone sensors: development and application of a Raspberry Pi-based UV camera*, Sensors, 16(10) (2016, October)1649.
Availabe: **https://doi.org/10.3390/s16101649**

[8] T. C. Krauss, S. C. Warlen, *The forensic science use of reflective ultraviolet photography*, Journal of Forensic Science, 30(1) (1985, January) 262-268.
Available: https://www.astm.org/jfs10991j.html

[9] C. Tetley, S. Young, *Digital infrared and ultraviolet imaging Part 1: infrared*, Journal of Visual Communication in Medicine, 30(4) (2007, July) 162-171.
Availabe: https://doi.org/10.1080/17453050701767106
[10] Z. Chen, P. Wang, B. Yu, *Research of UV detection system based on embedded computer*, In: 2008 World Automation Congress. IEEE, 2008, p. 1- 4.
Available: https://ieeexplore.ieee.org/abstract/document/4699210
[11] J. Fulton, E. James, *Utilizing the ultraviolet (UV detect) camera to enhance the appearance of photodamage and other skin conditions*, Dermatologic Surgery, 23(3) (1997, March) 163-169.
Available: https://doi.org/10.1111/j.1524-4725.1997.tb00013.x
[12] A. C. Vandaele, P. C. Simon, J. M. Guilmot, M. Carleer, R. Colin, *SO2 absorption cross section measurement in the UV using a Fourier transform spectrometer*, Journal of Geophysical Research: Atmospheres, 99(D12) (1994, December) 25599-25605.
Available: https://doi.org/10.1029/94JD02187
[13] T. Mori, M. Burton, *The SO2 camera: A simple, fast and cheap method for ground-based imaging of SO2 in volcanic plumes*, Geophysical research letters, 33(24) (2006, December) 1-5.
Available: https://doi.org/10.1029/2006GL027916
[14] T. P. Stecher, R. H. Cornett, M. R. Greason, W. B. Landsman, J. K. Hill, R. S. Hill, ... & W. H.Waller, *The ultraviolet imaging telescope: instrument and data characteristics*, Publications of the Astronomical Society of the Pacific, 109(735) (1997, May) 584-599.
Available: https://www.jstor.org/stable/40680932
[15] S. F. Cheak, *Detecting near-UV and near-IR wavelengths with the FOVEON image sensor*, Diss. Monterey California. Naval Postgraduate School, 2004.
Available: https://apps.dtic.mil/sti/citations/ADA429699
[16] https://patents.google.com/patent/US8289633B2/en
[17] N. Kaza, A. Ojaghi, F. E. Robles, *Ultraviolet hyperspectral microscopy using chromatic-aberration-based iterative phase recovery*, Optics letters, 45(10) (2020, May) 2708-2711.
Available: https://doi.org/10.1364/OL.392634
[18] W. J. Smith, *Modern optical engineering: the design of optical systems*, 4th Ed., McGraw-Hill Education, 2008.

Available: https://www.amazon.com/Modern-Optical-Engineering-4th-Ed/dp/0071476873

[19] I. H. Malitson, *A redetermination of some optical properties of calcium fluoride*, Applied Optics, 2(11) (1963, November) 1103-1107.
Available: https://doi.org/10.1364/AO.2.001103

[20] J. H. Burnett, Z. H. Levine, E. L. Shirley, *Intrinsic birefringence in calcium fluoride and barium fluoride*, Physical Review B, 64(24), (2001, November).
Available: https://doi.org/10.1103/PhysRevB.64.241102

[21] M .Dehghani, M. Hatami, A. Gharaati, *Supercontinuum Generation in Silica Plasmonic Waveguide by Bright Soliton*, Journal of Optoelectronical Nanostructures, 6(4) (2021) .
Available:10.30495/jopn.2022.28937.1236

[22] V. Fallahi, and M. Seifouri, *Novel structure of optical add/drop filters and multi-channel filter based on photonic crystal for using in optical telecommunication devices*, Journal of Optoelectronical Nanostructures, 4(2) (2019) 53-68.
Available: http://jopn.miau.ac.ir/article_3478.html

[23] H. Golamzadeh, R. Hosseini, H. Veladi, & H. Rahimi, *Amplification of Output Voltage by Using Silicon Based Solar Cells, Piezoelectric and Thermoelectric Conversion Transducers: A Triple Energy Harvester*, Journal of Optoelectronical Nanostructures, 8(2)(2023) 32-50.
Available: **10.30495/JOPN.2023.31481.1280**

[24] J. Noroz haghi, P. Aberoomand Azar, M. Saber Tehrani & S. Waqif Husain, *Preparation of Ionic Liquid-Silica Nanoparticles Nanocomposite Film Coated Porous Copper Wire for SolidPhase Microextraction of Pesticides from Tomato Samples*, Journal of Optoelectronical Nanostructures, 8(1)(2023) 58-83.
Available: 10.30495/JOPN.2023.30875.1269

[25] Parva, S., & M. HATAMI, *Nonlinear Energy Exchange Between Solitons In Modes Of A Silica Few-Mode Fiber*, Journal of Optoelectronical Nanostructures, 7(2) (2022) 63-78.
Available: **10.30495/JOPN.2022.29968.1259**

[26] N. Kristianpoller, I. KATZ, *Optical Properties of Various Types of Fused Silica*, JOSA, 60(3) (1970, March) 424-425.
Available: https://doi.org/10.1364/JOSA.60.000424

[27] https://www.earthwaterfire.com/optical/

[28] J. Sasián, *Introduction to lens design*, Cambridge University Press. (2019). Available: https://doi.org/10.1017/9781108625388
[29] R. Zemax, Zemax 13, *Optical Design Program*, User's Manual. (2014). Available: https://www.scribd.com/document/341465746/Zemax-Manual-pdf#
[30] J. Liu, J. Tan, T. Wilson, C. Zhong, *Rigorous theory on elliptical mirror focusing for point scanning microscopy*, Optics Express 20(6) (2012, March) 6175-6184.
Available: https://doi.org/10.1364/OE.20.006175